$(CH_3O)_2CH_2$ and to Dr. J. W. Downing for adapting the IGLO program.

Registry No. CH_3OH, 67-56-1; CH_3OCH_3, 115-10-6; $CH_3OCH_2OCH_3$, 109-87-5; $(CH_3O)_3CH$, 149-73-5; $(CH_3O)_4C$, 1850-14-2; $CH_3OS(O)OCH_3$, 616-42-2; CH_3CH_3, 74-84-0; $CH_3CH_2CH_3$, 74-98-6; $(CH_3)_3CH$, 75-28-5; $(CH_3)_4C$, 463-82-1; CH_3COCH_3, 67-64-1; CH_3CH_2OH, 64-17-5; $(CH_3CH_2)_2O$, 60-29-7; *cis*-$HCH_3C{=}CCH_3H$, 590-18-1; *trans*-$HCH_3C{=}CCH_3H$, 624-64-6; CH_3F, 593-53-3; CH_3SH, 74-93-1; $(CH_3)_2S$, 75-18-3; CH_3SSCH_3, 624-92-0; $CH_3SO_2CH_3$, 67-71-0.

Ultraviolet Resonance Raman Spectroscopy of Imidazole, Histidine, and Cu(imidazole)$_4^{2+}$: Implications for Protein Studies

Debra S. Caswell and Thomas G. Spiro*

Contribution from the Department of Chemistry, Princeton University, Princeton, New Jersey 08544. *Received February 6, 1986*

Abstract: Raman spectra have been obtained for aqueous imidazole, imidazolium, 4-methylimidazole, histidine, histidinium, and Cu(imidazole)$_4^{2+}$, with ultraviolet excitation at wavelengths from 229 to 200 nm provided by a H_2-Raman-shifted Nd:YAG laser. In every case, the excitation profiles show maxima at ~218 and ~204 nm, within the broad ~210-nm electronic absorption band. The two maxima are identified with the first two π–π^* transitions of the imidazole ring on the basis of the ring mode enhancement patterns. Substantial alterations of Raman-band frequencies and intensities are observed when the imidazole is protonated and/or substituted with a methyl group. The 4-methylimidazole spectra are similar to those of histidine. Coordination of Cu^{2+} to the imidazole has a smaller effect; several ring modes shift by a few wavenumbers. The imidazole(n) → Cu^{2+} charge-transfer transition is assigned near 240 nm on the basis of a Cu–N stretching mode enhancement similar to that of Cu(ethylenediamine)$_2^{2+}$ which has its charge-transfer band at this wavelength. Specific enhancement of a 950-cm^{-1} ring mode is also observed at 240 nm. Attempts to obtain RR spectra in the region (~300 nm) of the very weak imidazole(π) → Cu^{2+} charge-transfer transitions were unsuccessful. Although differences in the band positions might be used to distinguish protonated, unprotonated, and Cu-bound histidine residues in proteins, the overall enhancement is modest, and histidine signals are difficult to detect in the presence of the much larger signals from aromatic residues that are present in most proteins, as is illustrated in the case of the Cu protein stellacyanin.

It has recently become possible to obtain Raman spectra of biological molecules with excitation in the deep ultraviolet region via a pulsed Nd:YAG laser equipped with nonlinear optical frequency shifting devices.[1-3] Large resonance enhancements are seen for aromatic chromophores, such as the purine and pyrimidine bases of nucleic acids[4,5] and the phenylalanine, tyrosine, and tryptophan side chains of proteins,[6-8] as well as for the amide bands of the polypeptide chain.[6b,9] The imidazole ring of histidine also has π–π^* transitions in the deep UV and is a candidate for UV resonance enhancement. Histidine side chains of proteins play important roles as acid–base catalysts, and as ligands to protein-bound metal ions. It would therefore be of considerable interest to characterize the chemical environments of histidine using ultraviolet resonance Raman (UVRR) spectroscopy.

In this study we explore resonance effects in the deep UV (229–200 nm) Raman spectra of imidazole (ImH) and the imidazolium ion (ImH_2^+), of the Cu(ImH)$_4^{2+}$ complex, and of histidine (HisH), histidinium ($HisH_2^+$), and 4-methylimidazole (4-MeImH). Resonance enhancement of the imidazole ring modes is seen in each case, the intensity pattern varying with the excitation wavelength. Excitation profiles (EP's) in the 229–200-nm region show two distinct maxima, at ~218 and ~204 nm, for each of these molecules, although only a single broad absorption band peaking at ~207 nm is observed in solution. These EP maxima are identified with the first two imidazole π–π^* electronic transitions, on the basis of previously reported calculations;[10] the changes in the relative intensities of individual ring modes are consistent with these assignments. The data lend no support for assigning the ImH(n) → Cu charge-transfer (CT) transition at ~220 nm as previously proposed.[11] This transition is reassigned to an absorption shoulder at ~240 nm, similar in strength and wavelength to the CT band of Cu(en)$_2^{2+}$. RR spectra with 240-nm excitation show similar enhancements of the Cu–N breathing modes in the two complexes. Specific enhancement of a ImH ring mode, at 950 cm^{-1}, is also noted at this wavelength. Attempts to obtain Raman spectra in resonance with the very weak (ϵ ~ 300 M^{-1} cm^{-1}) ImH(π) → Cu CT transitions near 300 nm[11] were unsuccessful, the enhancement being too low.

Marked changes are seen in the vibrational frequencies among the imidazole derivatives. Although the Raman signature of the

(1) Ziegler, L. D.; Hudson, B. *J. Chem. Phys.* **1981**, *74*, 982.
(2) Asher, S. A.; Johnson, C. R.; Murtaugh, J. *Rev. Sci. Instrum.* **1983**, *54*, 1657.
(3) Fodor, S. P. A.; Rava, R. P.; Copeland, R. A.; Spiro, T. G. *J. Raman. Spectrosc.*, in press.
(4) (a) Ziegler, L. D.; Hudson, B.; Strommen, D. P.; Peticolas, W. L. *Biopolymers* **1984**, *23*, 2067. (b) Kubasek, W. L.; Hudson, B.; Peticolas, W. L. *Proc. Natl. Acad. Sci. U.S.A.* **1985**, *64*, 451.
(5) (a) Fodor, S. P. A.; Rava, R. P.; Hays, T. R.; Spiro, T. G. *J. Am. Chem. Soc.* **1985**, *107*, 1520. (b) Fodor, S. P. A.; Spiro, T. G. *Ibid.* **1986**, *108*, 3198.
(6) (a) Rava, R. P.; Spiro, T. G. *J. Am. Chem. Soc.* **1984**, *106*, 4062. (b) Rava, R. P.; Spiro, T. G. *Biochemistry* **1985**, *24*, 1861.
(7) Rava, R. P.; Spiro, T. G. *J. Phys. Chem.* **1985**, *89*, 1856.
(8) Johnson, C. R.; Ludwig, M.; O'Donnell, S.; Asher, S. A. *J. Am. Chem. Soc.* **1984**, *106*, 5008.
(9) (a) Copeland, R. A.; Spiro, T. G. *Biochemistry* **1985**, *24*, 4960. (b) Copeland, R. A.; Spiro, T. G. *J. Am. Chem. Soc.* **1986**, *108*, 1281.
(10) Bernarducci, E.; Bharadwaj, P. K.; Krogh-Jespersen, K.; Potenza, J. A.; Schugar, H. J. *J. Am. Chem. Soc.* **1983**, *105*, 3860.
(11) Fawcett, T. G.; Bernarducci, E. E.; Krogh-Jespersen, K.; Schugar, H. J. *J. Am. Chem. Soc.* **1980**, *102*, 2598.

0002-7863/86/1508-6470$01.50/0 © 1986 American Chemical Society

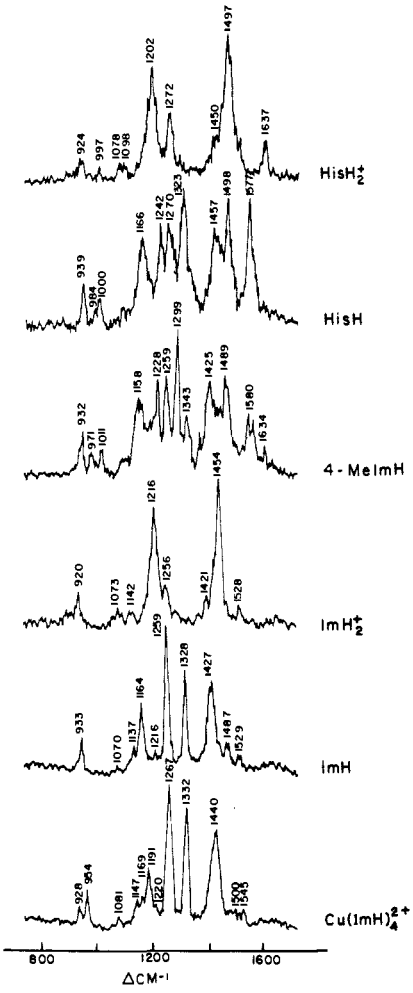

Figure 1. Raman spectra with 218-nm excitation for (top to bottom) histidinium (pH 4 phosphate buffer), histidine (pH 8 phosphate buffer), 4-methylimidazole (pH 8 phosphate buffer), imidazolium (pH 4 phosphate buffer), imidazole (pH 8 phosphate buffer), and the $Cu(ImH)_4^{2+}$ complex in water. Concentrations are ~10 mM (2.5 mM in Cu^{2+}). Peak frequencies (cm^{-1}) are marked.

histidine side chain is clearly sensitive to its chemical environment, the overall enhancement is modest. At wavelengths down to 200 nm, it is much less than the enhancement of phenylalanine, tyrosine, and tryptophan modes. Although some of the imidazole bands are well separated in frequency from interfering bands of the other aromatic residues, the relatively low enhancements make protein studies problematical. This is illustrated by RR spectra obtained at 218 nm for the Cu protein stellacyanin, and for a mixture of aromatic amino acids at concentrations corresponding to the protein composition. For this mixture, two histidine bands, identifiable via their pH dependence, can barely be detected, but they are lost in the noise of the protein spectrum.

Experimental Section

Imidazole, 4-methylimidazole, and $Cu(ClO_4)_2 \cdot 6H_2O$ (Aldrich) and the amino acids (Sigma) were used as purchased, except that the imidazole was sublimed twice and subsequently recrystallized three times, from distilled deionized water. Stellacyanin was isolated from Japanese lacquer acetone powder (Saito and Co., Ltd.) according to the method of Reinhammar.[12]

The imidazole derivatives and aromatic amino acids were dissolved in phosphate buffer at the concentrations indicated in the figure captions (4–5 mM for excitation profiles, 10–20 mM for displayed spectra). Histidine experiences UV photodecomposition after prolonged irradiation, and therefore this sample was changed after every scan (~12–20 min). Stellacyanin samples were replaced after every second scan. Sample integrity was monitored by the absence of time-dependent changes in the Raman spectra and of alterations in the UV absorption after Raman scans. The Raman spectra were checked at different laser power levels and showed no evidence of new peaks at higher power due to transient photoproducts.

The UV Raman apparatus is described in ref 3. UV excitation was provided by a pulsed Nd:YAG laser with a Raman shift cell operated with 3 atm of H_2 or 7 atm of D_2. The 532-, 355-, and 266-nm YAG harmonics were shifted by multiples of the 4155-cm^{-1} H_2 or 2993-cm^{-1} D_2 stretching frequencies. The following combinations were used: 532 nm + 6 and 7 ν_{H_2} (229 and 209 nm); 355 nm + 4 and 5 ν_{H_2} (223 and 204 nm); 266 nm + 0, 1, 2, and 3 ν_{H_2} (266, 240, 218, and 200 nm); and 266 nm + 3 ν_{D_2} (215 nm).

The laser beam intersected the sample in the free-jet portion (1-mm diameter) of a recirculating flow system containing 3–5 mL of sample. A 120° backscattering collection geometry was used. Raman intensities were measured relative to the O–H stretching band of solvent water for imidazole, imidazolium, and $Cu(ImH)_4^{2+}$ using absorption corrections as described in ref 5a. For histidine, phosphate ion was used as an internal standard. Intensities were measured relative to the 988-cm^{-1} HPO_4^{-2} band at pH 8 and the 879-cm^{-1} $H_2PO_4^-$ band at pH 4. The imidazole excitation profile was checked by using phosphate as an internal standard, and the same result was obtained as with the water band.

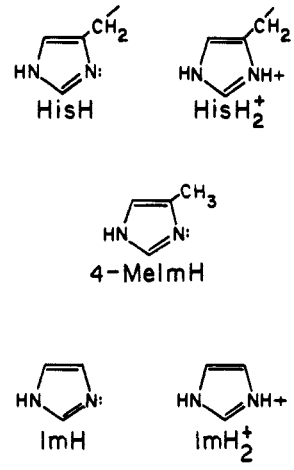

Figure 2. Structural diagrams for the imidazole derivatives included in this study.

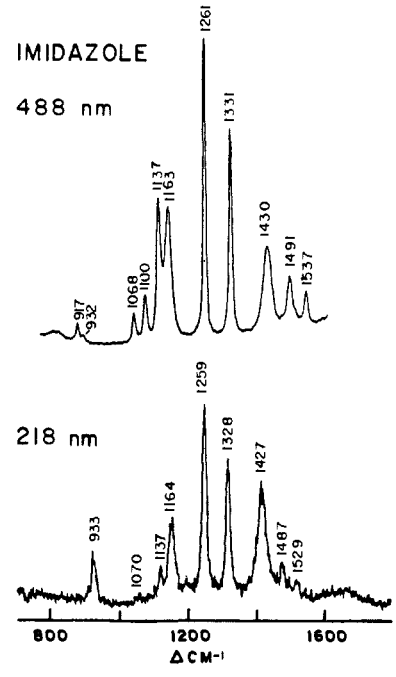

Figure 3. Raman spectra for aqueous imidazole with 218- (10 mM) and 488-nm (1 M) excitation.

Results and Discussion

A. Imidazole Ring Modes and Enhancement Patterns. Figure 1 compares resonance Raman spectra for imidazole (ImH) and a series of its derivatives (see structural diagrams in Figure 2),

(12) Reinhammar, B. *Biochim. Biophys. Acta* **1970**, *205*, 35.

Table I. Raman Frequencies (cm^{-1}) and Proposed Correlations for Imidazole Derivatives

assignment	ImH	$Cu(ImH)_4^{2+}$	ImH_2^+	4-MeImH	HisH	$HisH_2^+$
	917[a]	928	920			924
δ(R)	933	954		932	939	
				971	984	
				1011	1000	997
δ(R) + δ(C_2–H)	1070	1081	1073			1078
δ(R) + δ(C_4,C_5-H)	1100[b]	1107[b]				1098
δ(R) + δ(C_4,C_5-H)	1137	1147	1142			
δ(R) + δ(N_1-H)	1164	1191		1158	1166	
	1216	1220	1216	1228	1242	1202
δ(C_2–H)	1259	1267	1256	1259	1270	1272
δ(R)	1328	1332	1324[b]	1299	1323	
				1343	1351 (sh)	
δ(N_1–H)	1427	1440	1421	1425	1457	1450
δ(R) + δ(C_2-H)	1487	1500	1454	1489	1498	1497
δ(R) + δ(N_1-H)	1529	1545	1528			1536[b]
	1553[b]		1559[b]	1580	1577	
				1634		1637

[a] Observed with visible excitation. [b] Observed with 200-nm excitation.

obtained with 218-nm excitation, where the best quality spectra are obtained. The region 900–1650 cm^{-1} contains the in-plane ring modes which are prominent in both resonance and nonresonance Raman spectra. The intensity pattern at 218 nm is similar to that seen with 488-nm excitation[13] (Figure 3), suggesting preresonance with the first allowed π–π^* transitions as the dominant factor in the Raman intensities with visible wavelength excitation. Evidence for some contribution from higher lying transitions can also be seen, however, in the much higher relative intensities at 488 nm for bands at 1537, 1491, 1100, 1068, and 917 cm^{-1}; these appear weakly or not at all in the 218-nm RR spectrum. The imidazole mode frequencies and their assignments[13] are listed in Table I, along with suggested correlations for the ImH derivatives.

When ImH is bound to Cu^{2+} in the $Cu(ImH)_4^{2+}$ complex, the intensity pattern at 218 nm is preserved, but there is a systematic upshift, 5–20 cm^{-1}, in the ring mode frequencies. Thus a coordinate bond to Cu^{2+} produces a relatively modest perturbation of the electronic and vibrational properties of imidazole. When excess imidazole is present in the solution, several doublets can be seen clearly, due to the frequency differences, so that free and bound ImH are distinguishable in the RR spectrum. However, the enhancement factors are essentially the same for free and bound imidazole (vide infra) so that a small amount of bound imidazole cannot readily be detected in the presence of a large excess of unbound imidazole. The frequency shifts on binding are similar for Cu^{2+} and for Co^{2+},[13b] $Fe(CN)_5^{2-}$,[13a,14] or $Ru(NH_3)_5^{3+}$.[14]

Protonation of the imidazole ring (see ImH_2^+ spectrum in Figure 1) produces a much larger perturbation of the imidazole RR spectrum.[14,15] Only two strong bands now appear, at 1216 and 1454 cm^{-1}. This simplification is qualitatively consistent with the higher symmetry of the imidazolium ion. Protonation of imidazole raises the symmetry from C_s to C_{2v} and half of the ring modes (those with B_1 symmetry, which are antisymmetric with respect to the C_2 axis) are no longer subject to A term enhancement, the dominant mechanism in resonance Raman scattering.[20] This effect no doubt accounts for the disappearance of the 1164- and 1328-cm^{-1} bands which are prominent in the ImH spectrum. In addition the extra proton is expected to alter ring mode compositions via electronic and kinematic effects (The N–H in-plane bending coordinates mix with the ring modes). This may account for the replacement of the broad 1427-cm^{-1} band (probably containing more than one mode) and the weak 1487-cm^{-1} band in the ImH spectrum by the very strong 1454-cm^{-1} ImH_2^+ band with a low-energy shoulder and a remnant 1421-cm^{-1} band; the mixing among the three modes in this region evidently changes markedly upon protonation. Intensification of the 1216-cm^{-1} band in ImH_2^+ is also attributable to a change in the normal mode character.

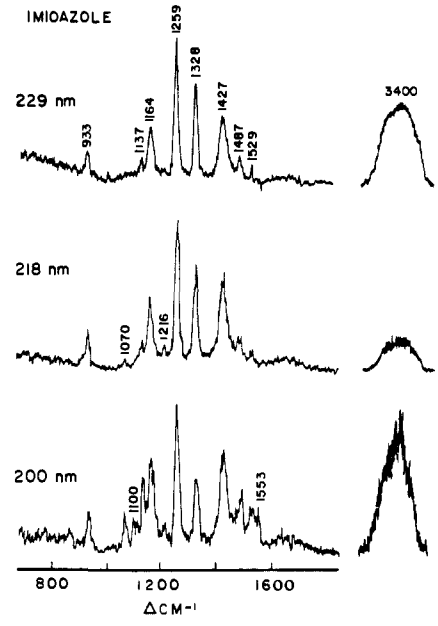

Figure 4. Raman spectra, at three deep-UV excitation wavelengths, for imidazole (10–15 mM in pH 8 phosphate buffer). The O–H stretching band of solvent H_2O, used as an intensity standard, is shown on the same scales; its apparent intensity varies with the scaling factor used to keep the imidazole intensities comparable.

Substitution of a methyl group on the ring also produces a marked change in the ring modes, as seen in the RR spectrum of 4-methylimidazole, shown in Figure 1. The spectrum is much richer, and although counterparts can be seen for all of the ImH bands, their frequencies and intensities are altered significantly, and several new bands make an appearance. Substitution of H by CH_3 on a ring carbon atom replaces one kind of kinematic interaction of the ring modes (with in-plane C–H bending) with others (C–CH_3 stretching and C–C–H bending), and also alters the electronic properties of the ring somewhat (electron donation from the methyl group). 4-MeImH was chosen as a mimic for histidine, the 4-methyl group substituting for the histidine methylene group, attached to the amino acid C_α carbon atom (Figure 2). Indeed the histidine RR spectrum (see HisH spectrum in Figure 1) resembles that of 4-MeImH quite closely in its intensity pattern, yet there are significant frequency shifts for most of the band frequencies. These changes presumably result mainly from the kinematic differences between a methyl group and a methylene group and the resultant alteration in the ring mode

(13) (a) Walters, M. A.; Spiro, T. G. *Inorg. Chem.* **1983**, *22*, 4014. (b) Salama, S.; Spiro, T. G. *J. Am. Chem. Soc.* **1978**, *100*, 1105.
(14) Jones, C. M.; Johnson, C. R.; Asher, S. A.; Shepherd, R. E. *J. Am. Chem. Soc.* **1985**, *107*, 3772.
(15) Yoshid, C. M.; Friedman, T. B.; Loehr, T. M. *J. Am. Chem. Soc.* **1975**, *97*, 1028.

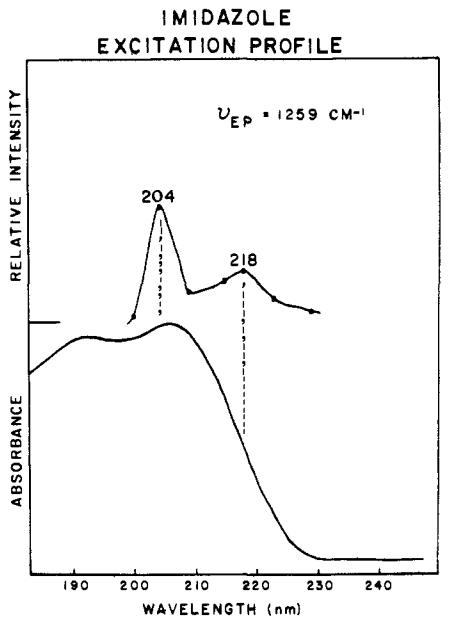

Figure 5. Excitation profile for the 1259-cm^{-1} band of aqueous imidazole, compared with the absorption spectrum. See Experimental Section for details of the measurement.

interactions. Thus the imidazole RR spectrum is surprisingly sensitive to the exact nature of peripheral substituents. When histidine is protonated (see $HisH_2^+$ in Figure 1), there is again a dramatic simplification of the spectrum.[16,17] As in the case of ImH_2^+, two bands are dominant at 1202 and 1497 cm^{-1}; evidently the imidazolium ring on $HisH_2^+$ has quasi-C_{2v} symmetry, despite the presence of the methylene substituent.

B. π-π^* Resonance Enhancement. Figure 4 shows RR spectra of imidazole with 200-, 218-, and 229-nm excitation and the 3400-cm^{-1} OH stretching band of the solvent H_2O, which serves as an internal standard. It is evident that both the overall enhancement and the relative intensities of the individual bands vary with excitation wavelength. In Figure 5 the excitation profile (EP) of the strong 1259-cm^{-1} band is compared with the imidazole absorption spectrum. Two broad absorption bands are seen, the lower energy one peaking at ~207 nm. This wavelength is at a minimum with the Raman EP, however, which shows two flanking peaks, at ~204 and ~218 nm. (Although the excitation profile is at low resolution and these wavelengths are inexact, they are nevertheless reasonably well defined by the available points.) The frequency difference between the EP peaks, ~3100 cm^{-1}, is much larger than any of the imidazole ring frequencies, and assignment to a 0, 0/0, 1 vibrational sequence in the excited state is therefore precluded. We infer that the peaks correspond to two electronic transitions, both of which are contained within the broad ~207-nm absorption band envelope.

The valence orbitals of imidazole include the n orbital, containing the unprotonated N lone pair, and two π orbitals, π_1 and π_2, which are mainly C and N based (Figure 6).[18] There are two corresponding π^* orbitals which are the lowest unfilled orbitals of imidazole. The lowest lying electronic transitions are therefore expected to include two n-π^* and four π-π^* transitions. Two calculations of the expected transition energies have been carried out, at CNDO/S[18] and INDO/S[10] levels. The more recent INDO/S calculation predicts the n-π^* transitions at 284 and 213 nm, and the first two π-π^* transitions at 226 and 199 nm.[10] The n-π^* transitions, being symmetry forbidden, are expected to have zero oscillator strength and small if any contribution to the Raman intensities, via vibronic coupling.[19] We note that the Raman EP

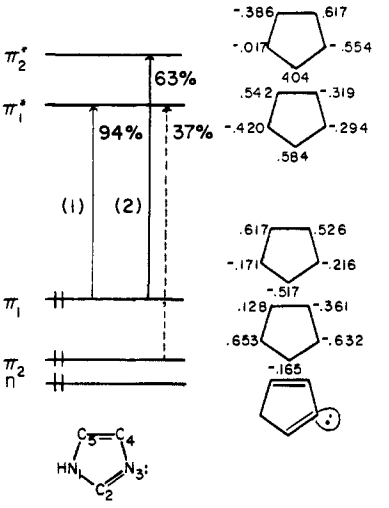

Figure 6. Orbital energy diagram with MO coefficients of Del Bene and Jaffé[18] for imidazole. Contributions to the lower energy (1) and higher energy (2) $\pi \rightarrow \pi^*$ transitions are displayed.

Table II. Change in Bond Orders for the Indicated Orbital Excitations[a]

bond	$\pi_1 \rightarrow \pi_1^*$	$\pi_1 \rightarrow \pi_2^*$	$\pi_2 \rightarrow \pi_1^*$	$\pi_2 \rightarrow \pi_2^*$
N_1-C_5	0.12	0.11	0.32	0.08
N_3-C_4	0.02	0.23	0.14	0.57
N_1-C_2	0.32	0.10	0.13	0.10
C_4-C_5	0.50	0.56	0.13	0.20
N_3-C_2	0.31	0.36	0.28	0.33

[a] Calculated from the CNDO/S MO coefficients of Del Bene and Jaffe.[18]

peaks correspond quite well to the INDO/S predictions for the first two π-π^* transitions. Assuming that the lowest π-π^* transition corresonded to the 207-nm peak in the absorption spectrum, Schugar and co-workers corrected all of their INDO/S energies by adding 0.5 eV to them.[10] This becomes unnecessary if we assume that the transition energies are correctly given by the Raman EP's, the transitions being unresolved in the broad absorption band. The earlier CNDO/S predictions do, however, require adding 0.5 eV to bring the first two π-π^* transitions, calculated at 248 and 221 nm,[18] into line with the EP maxima. The present data are an interesting example of the better resolution of electronic states that can often be obtained from Raman EP's.

The composition of the lowest π-π^* transition is calculted[18] to be almost entirely due to the π_1-π_1^* orbital excitation (94%), while the second transition is 63% $\pi_1 \rightarrow \pi_2^*$ and 37% $\pi_2 \rightarrow \pi_1^*$ (see 1 and 2 in Figure 6). Table II gives bond-order changes for the ring bonds calculated for the π-π^* orbital excitations, with the orbital coefficients in ref 18. These can be used, in connection with the normal mode compositions to anticipate the Raman enhancement patterns for the π-π^* transitions. The relative enhancements depend on the extent to which the excited-state potential is shifted along the individual normal modes.[20] Resonance with the first π-π^* transition should give maximal enhancement to those modes with largest contributions from C_4-C_5, N_1-C_2, and N_3-C_2 bond stretching since these bonds undergo the largest change for the $\pi_1 \rightarrow \pi_1^*$ excitation. On the other hand, C_4-C_5 shows the largest change for $\pi_1 \rightarrow \pi_2^*$, which makes up 67% of the second π-π^* transition, and N_3-C_4 and N_3-C_2 are also important; N_1-C_5 and N_3-C_2 contribute through the 37% $\pi_2 \rightarrow \pi_1^*$ character.

In Table III, the imidazole Raman bands are listed in order of increasing intensity ratio for 218 vs. 200-nm excitation, these wavelengths being close to resonance with the first two π-π^* transitions, according to our interpretation of the EP's. The ratios range from 0.2 to 5.6, a factor of 28 variation. Modes at the top and bottom of the list are preferentially enhanced via the higher

(16) Chinsky, L.; Jolles, B.; Laigle, A.; Turpin, P. Y. *J. Raman Spectrosc.* **1985**, *16*, 239.
(17) Hudson, B.; Mayne, L. In *Methods in Enzymology*, in press.
(18) Del Bene, J.; Jaffé, H. H. *J. Chem. Phys.* **1968**, *48*, 4050.
(19) Kamagawa, K.; Ito, M. *J. Mol. Spectrosc.* **1976**, *60*, 277.
(20) Spiro, T. G.; Stein, P. *Annu. Rev. Phys. Chem.* **1977**, *28*, 501.

Table III. Imidazole Modes Listed in Order of Their RR Enhancement at 218 vs. 200 nm

ν_{ImH} (cm^{-1})	intensity[a] 218/200	potential energy distribution[b,c] (%)					
1070	0.21	29	N_1–C_5 N_3–C_4	18	(N_1–C_2)	14	(C_4–C_5)
1100	0.26	25	N_1–C_5 N_3–C_4				
1137	1.57	9	N_1–C_5 N_3–C_4				
1529	1.74	19.5	N_1–C_5 N_3–C_4			8	(C_4–C_5)
1487	2.24	30	N_1–C_5 N_3–C_4	18	(N_1–C_2)		
933	2.65	19	N_1–C_5 N_3–C_4			10	(C_4–C_5)
1164	3.18						
1427	3.87					23	(C_4–C_5)
1259	4.05	4	N_1–C_5 N_3–C_4	4	(N_1–C_2)	9	(C_4–C_5)
1328	5.63	21	N_1–C_5 N_3–C_4	33	(N_1–C_2)		

[a] Intensity ratio 218/200 nm normalized to 3400-cm^{-1} H_2O band. [b] Contributions (%) from stretching of the indicated bonds (see Figure 6). [c] $\nu(N_3$–$C_2)$ contributions not shown since approximately same ΔBO for all transitions (~ 0.32).

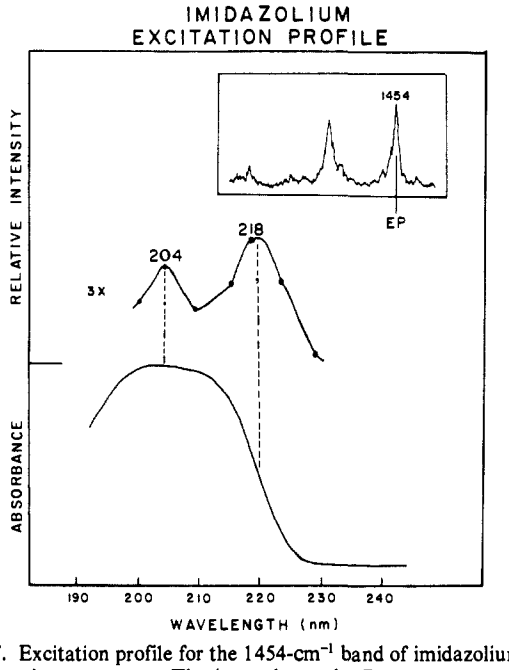

Figure 7. Excitation profile for the 1454-cm^{-1} band of imidazolium, and the absorption spectrum. The inset shows the Raman spectrum with 218-nm excitation.

and lower of the two π–π^* transitions, respectively. Also listed are the potential energy distributions for the normal modes as obtained form the calculations of Colombo et al.[21] While the internal coordinate contributions are substantially mixed in the potential energy distribution, it is evident that the modes at the top of the list have major contributions from N_1–C_5 and N_3–C_4 stretching, which are involved in the higher π–π^* transition primarily. Modes at the bottom of the list have larger contributions either from C_4–C_5 stretching or N_1–C_2 stretching, both of which are expected to be important in the lower π–π^* transition. Thus, the enhancement pattern is at least qualitatively in accord with the two excitation profile assignments. A similar intensity analysis has been given by Jones et al.[14] for ImH enhancements in resonance with charge-transfer transitions of $Fe(CN)_5(ImH)^{2-}$.

Figures 7, 8, and 9 show excitation profiles for ImH_2^+, HisH, and $HisH_2^+$, respectively; the band being monitored is shown in the inset RR spectra. Although the shape of the absorption spectra differ appreciably, two excitation profile peaks are always seen, near 204 and 218 nm. The wavelength maxima vary slightly, as do the relative amplitudes of the two peaks. The similarity is striking, however. It is evident that the same electronic transitions are involved in each case, and that the changes in the RR spectra of these species are due to altered normal mode compositions and symmetries in the ground state. The absence of any major effect associated with protonation of the imidazole ring strengthens the view that n → π^* transitions do not contribute significantly to the Raman scattering, since these transitions are shifted to much

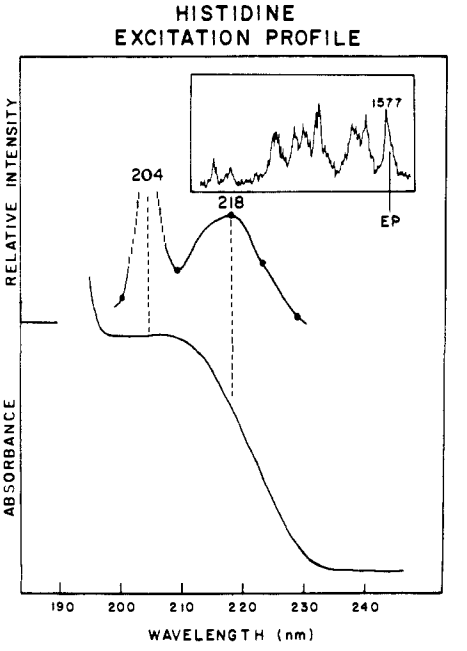

Figure 8. Excitation profile for the 1577-cm^{-1} band of histidine, and the absorption spectrum. The inset shows the 218-nm excited Raman spectrum. The intensity at 204 nm is unavailable because of poor signal to noise in the region of the intensity standard for this sample.

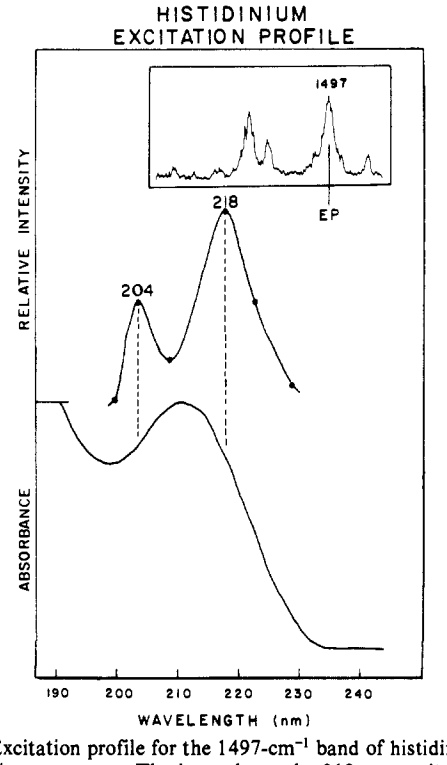

Figure 9. Excitation profile for the 1497-cm^{-1} band of histidinium, and the absorption spectrum. The inset shows the 218-nm excited Raman spectrum.

(21) Columbo, L.; Bleckman, P.; Schrader, B.; Schneider, R.; Plesser, Th. *J. Chem. Phys.* **1974**, *61*, 3270.

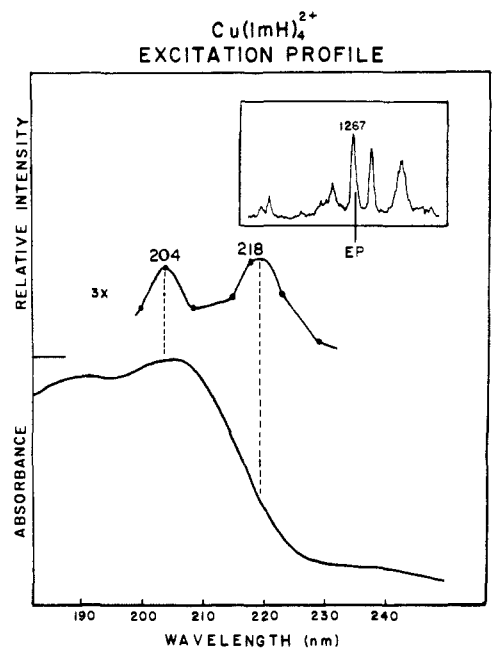

Figure 10. Excitation profile for the 1267-cm^{-1} band of $Cu(ImH)_4^{2+}$, and the absorption spectrum. The inset shows the 218-nm excited Raman spectrum.

higher energy by protonation of the nitrogen lone pair.

C. π–π^* and Charge-Transfer Transitions in $Cu(ImH)_4^{2+}$. Figure 10 shows the absorption spectrum and excitation profile for $Cu(ImH)_4^{2+}$. Once again two profile maxima are observed, near 204 and 218 nm, which are within the broad absorption band at ~207 nm. The profile resembles that of ImH_2^+ more closely than that of ImH itself. For both ImH_2^+ and $Cu(ImH)_4^{2+}$ the lower energy (EP) peak is slightly redshifted (~220 nm) and is stronger relative to the corresponding ImH peak. These differences suggest a small and comparable polarization effect of H^+ and Cu^{2+} on the imidazole π–π^* transition moments.

Schugar and co-workers[10,11,22] analyzed the absorption spectrum of $Cu(ImH)_4^+$ as well as of other imidazole complexes in solution and in polycrystalline samples. They concluded that the 207-nm absorption band contained both ImH π–π^* and ImH(n) → Cu charge-transfer transitions. A principal reason for this assignment was their finding of a molar extinction coefficient for $Cu(ImH)_4^{2+}$ of 41 000 at 207 nm, while a value of 27 600 would have been expected from the imidazole π–π^* absorption alone (6900 per ImH). In our hands, however, the 207-nm extinction coefficient was consistently 21 000, essentially four times the value we observed for imidazole (5000). (This result was obtained in both aqueous and methanolic solutions, using the same concentrations, 0.0014 M ImH and 0.0035 M Cu^{2+}, as Schugar and co-workers, and 100-μ path-length absorption cells. At this concentration $Cu(ImH)_4^{2+}$ ligand dissociation is estimated[22] to be less than 10%.) We have no explanation for this discrepancy. In addition Schugar and co-workers found two absorption bands in mull spectra of polycrystalline Cu–imidazole complexes, at 204 and 220 nm, and assigned these to ImH π–π^* and ImH(n) → Cu charge-transfer transitions, respectively.[11] These two absorption maxima correspond very well to our ImH excitation profile peaks, which are present whether Cu^{2+} is bound or not. Consequently we conclude that the 204- and 220-nm absorption peaks seen by Schugar and co-workers are the two first π–π^* transitions of ImH, which are resolved in the polycrystaline samples but not in solution. There is no evidence, either from the Raman enhancement and excitation profiles, or, in our hands, from the extinction coefficients, for a contribution in this region from ImH → Cu charge transfer.

If the ImH(n) → Cu charge-transfer transition is not in the 200–220-nm region, where is it? $Cu(ImH)_4^{2+}$ shows an absorption shoulder of moderate intensity ($\epsilon \sim 3500$ M^{-1} cm^{-1}) at 240 nm (see Figure 10). These characteristics are similar to those of the σ charge-transfer band ($\lambda \sim 240$ nm) of $Cu(en)_2^{2+}$ (en = ethylenediamine).[23] A ligand(σ) → metal charge-transfer transition is expected to produce enhancement of the metal–ligand stretching vibration. For $Cu(en)_2^{2+}$ the Cu–N breathing mode is expected at ~415 cm^{-1}.[24] We located this band in the RR spectrum (not shown) of $Cu(en)_2^{2+}$ excited at 240 nm, and found it to have a modest enhancement, 6.2 times the intensity of the SO_4^{2-} breathing mode at 983 cm^{-1} on a molar basis, consistent with the relatively low oscillator strength of the electronic transition. For $Cu(ImH)_4^{2+}$ we were likewise able to locate the Cu–ImH breathing mode, at 245 cm^{-1},[25] in the 240-nm RR spectrum, although the rising background from the Rayleigh line (the single monochromator used for these spectra has limited stray light rejection) degraded the signal quality. Nevertheless, we were able to estimate an enhancement factor relative to the SO_4^{2-} breathing mode of ~8, similar to the value found for the $Cu(en)_2^{2+}$ breathing mode. These intensity measurements were replicable in repeated experiments. Schugar and co-workers[11] argued that the σ CT transition should be ~5000 cm^{-1} higher for ImH then en, based on the free ligand ionization potentials. The effects on these energies of bonding to Cu^{2+} are, however, unknown. In null spectra of polycrystalline $Cu(ImH)_4^{2+}$ pairs of bands were seen at 240/260 and 305/335 nm, which were assigned to CT transitions from the ImH π_1 and π_2 orbitals, the splitting being attributed to different orientations of the ImH rings.[11] In solution, these discrete bands are replaced with broad weak ($\epsilon \sim 300$) absorption over the 260–340-nm range, which presumably contains both π CT transitions, the breadth being attributable to a distribution of ImH orientations.[11] In the case of $Fe(CN)_5(ImH)^{2-}$ bands in the 400–480-nm region have been suggested[13a,14] to contain the π-charge transfers, on the basis of differential exci-

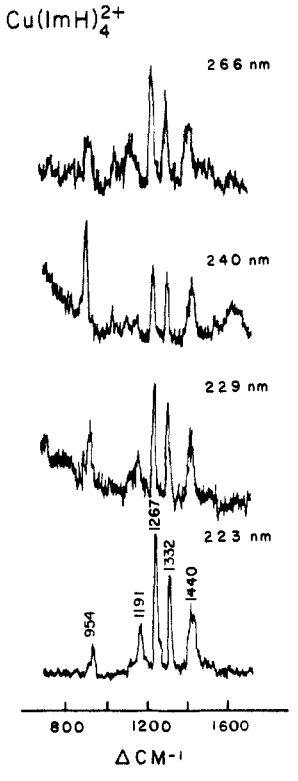

Figure 11. Raman spectra of $Cu(ImH)_4^{2+}$ (5 mM in copper) excited at wavelengths above the strong π–π^* absorption. Note the dominance of the 954-cm^{-1} band at 240 nm, suggested due to a proposed resonance with the ImH(n) → Cu CT transition.

(22) Bernarducci, E.; Schwindinger, W. F.; Hughey, J. L., IV.; Krogh-Jespersen, K.; Schugar, H. J. *J. Am. Chem. Soc.* **1981**, *103*, 1686.

(23) Miskowski, V. M.; Thich, J. A.; Solomon, R.; Schugar, H. J. *J. Am. Chem. Soc.* **1976**, *98*, 8344, and references cited therein.

(24) Lever, A. B. P.; Mantovani, E. *Inorg. Chem.* **1971**, *10*, 817.

(25) Larrabee, J. A.; Spiro, T. G. *J. Am. Chem.* **1980**, *102*, 4217.

tation profiles. The Fe–ImH stretching mode was extremely weak in these spectra.[13a,14] We suggest that the ~240-nm band of $Cu(ImH)_4^{2+}$ is due to the σ charge transfer while both π charge transfers contribute to the broak weak 260–340-nm band.

The ring mode enhancement pattern is expected to show differential effects for charge-transfer resonances.[13a,14] That this is the case for the 240-nm transition is clearly shown by Figure 11, in which $Cu(ImH)_4^{2+}$ Raman spectra are compared for 223-, 229-, 240-, and 266-nm excitation. The overall scattering becomes steadily weaker in this series as the preresonance effects of the intense π–π^* transitions diminish, but a relative augmentation is seen for the 954-cm^{-1} band, which becomes the strongest feature of the 240-nm spectrum. In a separate experiment, the intensities of the 954-cm^{-1} and also of the 1267-cm^{-1} band, which was the strongest feature in the π–π^* resonance enhanced spectrum, were measured relative to the 983-cm^{-3} sulfate band, present as an internal standard. The molar enhancement factors for the 954- and 1267-cm^{-1} bands were 34.6 and 69.1 at 229 nm, 29.5 and 21.4 at 240 nm, and 6.2 and 6.9 at 266 nm. Although the enhancement factors for both bands decrease continuously with increasing energy separation from the π–π^* transitions, the 954/1267 cm^{-1} ratio reaches a maximum at 240 nm, reflecting a local resonance with the charge-transfer transition. The 954-cm^{-1} band is assigned[21] as a deformation mode of the imidazole ring. Evidently this mode is specifically coupled to the excitation of the σ electrons on the imidazole N atom which is bonded to Cu.

Resonance with the ImH(π) → Cu charge-transfer transitions is expected to involve a further alteration in the ring mode enhancement pattern. In the case of $Fe(CN)_5(ImH)^{2-}$ the π charge-transfer enhancement was found to favor the 1330-cm^{-1} band, which became the strongest one in the spectrum, while the normally strong 1267-cm^{-1} band became quite weak.[13a,14] The overall enhancement was low, however, the 1330-cm^{-1} band being only 4.1 times as strong as the 983-cm^{-1} band of SO_4^{2-}.[13a] We tried to record the $Cu(ImH)_4^{2+}$ RR spectrum with 282-nm excitation, but were unable to obtain an adequate signal to determine the intensity pattern. The enhancement factor is too low to obtain acceptable spectra under current experimental conditions.

D. Implications for Protein Studies. The RR spectrum of histidine could in principle play a useful role in protein structural studies, because of the sensitivity of the vibrational frequencies to the chemical environment of the imidazole. Imidazole protonation produces dramatic effects on the Raman spectrum, and coordination to metal ions induces readily discernible shifts in the ring mode frequencies. Even a shift to the N3 tautomer of histidine, which can be induced by H-bonding in proteins, is known[26] to produce distinctive changes in the vibrational spectrum.

Unfortunately, the utility of the histidine RR spectrum for protein studies is severely limited by low sensitivity. Although resonance enhancement via the π–π^* transitions is appreciable, it is much lower than the enhancement seen for the aromatic side chains, phenylalanine, tyrosine, and tryptophan.[7] This is illustrated in Table IV, where molar enhancement factors, relative to H_2O, are listed for prominent bands of the aromatic amino acids for excitation at 200, 218, and 240 nm (wavelengths at which excitation is most easily produced with the H_2-Raman shifted YAG laser). Both histidine and tryptophan are maximally enhanced at 218 nm, but the scattering cross section for tryptophan is an order of magnitude higher. The lower scattering efficiency of histidine can be traced directly to the smaller transition moment for its π–π^* transition. The molar absorptivity is 5000 for histidine at its 207-nm maximum, but 36 000 for tryptophan at its 220-nm maximum. To a first approximation the resonance enhancement scales with the square of the transition moment[20] so that an ~50-fold lower enhancement (on the rough approximation that the transition moment is proportioned to the molar absorptivity) is expected for histidine relative to tryptophan. The actual intensity ratio with 218-nm excitation is ~16 for the 1016-cm^{-1} Trp band to the 1575-cm^{-1} HisH band. In view of the very different character of the electronic and vibrational states involved in this comparison, the correspondence is not unreasonable. For tyrosine and phenylalanine, 218 nm is in the region of quasi-forbidden electronic transitions, and the scattering is preresonantly enhanced, as well as vibronically induced.[7] Nevertheless, the enhancement factors are still three-fold to four-fold higher than for histidine. Consequently histidine is expected to show up weakly or not at all in protein RR spectra at wavelength down to 200 nm. None of the protein spectra published to date show any positive evidence for histidine.

To illustrate the sensitivity required, we show in Figures 12 and 13 the 218-nm excited RR spectra of the copper protein stellacyanin, as well as that of a mixture of histidine, phenylalanine,

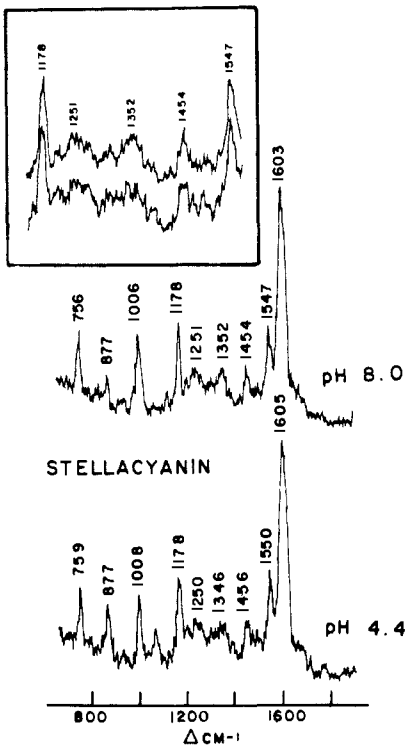

Figure 12. Raman spectra with 218-nm excitation for stellacyanin (0.33 mM) at pH 8.0 (phosphate buffer) and pH 4.4 (phosphate buffer). The inset is a blow-up of the 1100–1550-cm^{-1} region, where histidine bands might be detected by their pH sensitivity, but are not.

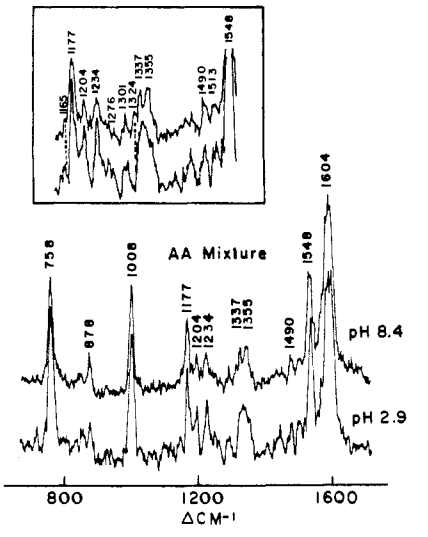

Figure 13. Raman spectra with 218-nm excitation for a solution containing histidine and the aromatic amino acids in the same molar proportions (0.44, 0.56, 0.78, and 0.33 mM for histidine, phenylalanine, tyrosine, and tryptophan) as in the stellacyanin solution of Figure 12, at pH 8.4 (phosphate buffer) and 2.9 (phosphate buffer). The inset shows bands at 1165 and 1324 cm^{-1} assignable to histidine modes via their disappearance at pH 2.9.

(26) Ashikawa, I.; Itoh, K. *Biopolymers* **1979**, *18*, 1859.

Table IV. Molar Enhancement Factors ($X10^{-2}$)[a] for Selected Raman Bands of the Aromatic Amino Acids[b] at the Indicated Excitation Wavelengths

	tryptophan	tyrosine	phenylalanine	histidine
selected band (cm^{-1})	1016	1617	1000	1575
200 nm	29	202	36	8
218 nm	506	126	96	32
240 nm	53	30	8	4

[a] Measured relative to the 3400 cm^{-1} H_2O Raman band. See ref 5a for details of the calculation. [b] Values for tryptophan, tyrosine, and phenylalanine from ref 7.

tyrosine, and tryptophan at concentrations which are the same as those of the amino acid constituents of the stellacyanin solution. Stellacyanin contains five phenylalanine, seven tyrosine, three tryptophan, and four histidine residues;[27] two of the histidine imidazoles are believed to be coordinated to the single Cu atom in the protein.[28] At this wavelength the spectrum is dominated by tryptophan bands. It is possible to discern histidine bands at 1165 and 1324 cm^{-1} in the amino acid mixture (Figure 13; see inset) because they are eliminated at low pH, as expected from the spectrum of $HisH_2^+$ (see Figure 1). They are extremely weak, however, and the remaining HisH bands are covered up by bands from the other amino acids, as are all the $HisH_2^+$ bands at low pH. The stellacyanin spectra (Figure 12) show no pH-associated changes that can be attributed to histidine. (Minor changes can be seen in tryptophan bands at 877 and 1350 cm^{-1}, which may be due to altered solvent exposure).[6b] Even the 1165- and 1324-cm^{-1} HisH bands detectable in the spectrum of the amino acid mixture are lost in the noise for stellacyanin. We conclude that the prospects are not good for monitoring histidine in proteins via RR spectroscopy at the currently available UV wavelengths.

Acknowledgment. We thank Professor Harvey Schugar for helpful discussions. This work was supported by NIH Grant GM13498.

Registry No. ImH, 288-32-4; ImH_2^+, 17009-90-4; 4-MeImH, 822-36-6; HisH, 71-00-1; $HisH_2^+$, 70805-60-6; $Cu(ImH)_4^{2+}$, 24349-51-7.

(27) Bergman, C.; Candrik, E. K.; Nyman, P. O.; Strid, L. *Biochem. Biophys. Res. Commun.* **1977**, *77*, 1052.

(28) Peisach, J.; Powers, L.; Blumberg, W. E.; Chance, B. *Biophys. J.* **1982**, *38*, 277.

Measurement of Deuterium Kinetic Isotope Effects in Organic and Biochemical Reactions by Natural Abundance Deuterium NMR Spectroscopy

Robert A. Pascal, Jr.,* Mary W. Baum, Carol K. Wagner,[1] Lauren R. Rodgers, and Ded-Shih Huang

Contribution from the Department of Chemistry, Princeton University, Princeton, New Jersey 08544. *Received March 18, 1986*

Abstract: Natural abundance deuterium NMR spectroscopy is a powerful and convenient tool for the estimation of deuterium kinetic isotope effects in organic reactions, obviating in many cases the preparation of isotopically enriched reactants for such measurements. Determinations of the primary or secondary kinetic isotope effects for a broad variety of reaction types are described to illustrate this technique.

Molecules enriched with isotopes of hydrogen are often employed in the diagnosis of reaction pathways in organic chemistry and biochemistry.[2] The isotopic label must be present in quantities great enough to permit easy detection, and, in most circumstances, a knowledge of the location of the isotope in the starting material and product(s) is essential for the correct interpretation of the experiments performed. Unfortunately, the most commonly used methods for detection of deuterium (mass spectrometry) and tritium (liquid scintillation counting), while very sensitive, do not usually permit the unambiguous assignment of the precise sites of isotopic substitution. For this reason, the synthesis of organic compounds specifically labeled with deuterium or tritium has become a frequently necessary if laborious task for the mechanistic chemist or biochemist. However, deuterium is present at low concentrations (~0.015%)[3] in all ordinary hydrogen-containing compounds. A satisfactory method for quantitation of this isotope at each site in a molecule would eliminate, in many cases, the requirement for specific isotopic enrichment.

In fact the great sensitivity and chemical shift dispersion achievable with modern high field NMR instrumentation permit the relatively easy assessment of the amount of deuterium at specific molecular sites, and it is now possible to employ deuterium at natural abundance as an isotopic tracer, with detection of the tracer by ^2H NMR spectroscopy. By using this method Martin et al.[4] have shown that there can be dramatic variations in the deuterium distributions within identical compounds from different sources. These variations must reflect the differing chemical histories of these molecules as illustrated for anethole samples[5a] and for camphor samples[5b] of natural and synthetic origins. Martin's group has further demonstrated the feasibility of using these variations from the statistical abundance of deuterium for determination of the origin of alkyl groups in organic reactions.[6] In this paper we explore the use of natural abundance deuterium NMR for the measurement of kinetic isotope effects (KIE's) in organic reactions.[7]

(1) Visiting Professor from the Department of Chemistry, Rutgers University, New Brunswick, NJ 08903.

(2) Several excellent reviews are found in: *Isotopes in Hydrogen Transfer Processes*; Buncel, E., Lee, C. C., Eds.; Elsevier: New York, 1976.

(3) Garson, M. J.; Staunton, J. *Chem. Soc. Rev.* **1979**, *8*, 539–561.

(4) Martin, G. J.; Martin, M. L. *Tetrahedron Lett.* **1981**, *22*, 3525–3528.

(5) (a) Martin, G. J.; Martin, M. L.; Mabon, F.; Brieout, J. *J. Am. Chem. Soc.* **1982**, *104*, 2658–2659. (b) Grant, D. M.; Curtis, J.; Croasmun, W. R.; Dalling, D. K.; Wehrli, F. W.; Wehrli, S. *J. Am. Chem. Soc.* **1982**, 104, 4492–4494.

(6) Martin, G. J.; Martin, M. L.; Mabon, F.; Michon, M.-J. *J. Chem. Soc., Chem. Commun.* **1982**, 616–617.

0002-7863/86/1508-6477$01.50/0 © 1986 American Chemical Society